AIAA-2002-5733

Finite Element Model of Fluid Flow Inside a Micro-Thruster

Reni Raju, B.P. Pandey and Subrata Roy
Computational Plasma Dynamics Laboratory
Kettering University
Flint, MI 48504

NanoTech 2002 - "At the Edge of Revolution"
9 - 12 Sep 2002
Houston, Texas

Finite Element Model of Fluid Flow inside a Micro-Thruster

Reni Raju[*], **B.P. Pandey**[†] and **Subrata Roy**[‡]
Computational Plasma Dynamics Laboratory
Department of Mechanical Engineering
Kettering University, Flint, Michigan 48504, USA

Microchannel based propulsion systems have come in handy in development of precise control and maneuvering of small spacecrafts. However it is difficult to predict the performance of the microthrusters numerically since the standard assumptions of using Navier Stokes equations break down at micro scale. A two-dimensional finite element based macroscopic model is currently being developed to incorporate the effect of slip boundary conditions as well as transition regime for reasonably high Knudsen number flow inside a micro-thruster. This paper documents the status of this development and will address relevant numerical issues. As a first case, a Si-micromachined solid propellant based converging-diverging microthruster nozzle, manufactured at LAAS-CNRS, is modeled for high temperature application using no-slip continuum. While the 2-D results obtained by this simulation are comparable to the 1-D results published in the literature, the 2-D model shows better flow details and predicts significantly higher thrust. The model is further examined for a cold microthruster of similar nozzle geometry by implementing the slip wall boundary with temperature jump wall condition for higher Knudsen Number.

Nomenclature

α	Nozzle divergence angle
A_1	Cross-sectional area of the chamber
A_2	Cross-sectional area of the throat
C_p	Specific heat at constant pressure
Ec	Eckert number
γ	Specific heat ratio
ℓ	Mean free path of the fluid
L_1	Length of the chamber
L_2	Length of the converging part of the nozzle
L_3	Length of the diverging part of the nozzle
Kn	Knudsen Number
Ma	Mach number
μ	Coefficient of viscosity
Pr	Prandtl number
P	Gas pressure
P_0	Reference pressure
ρ	Gas density
ρ_0	Reference density
ρ_p	Propellant density
R	Reduced gas constant
Re	Reynolds number
σ_v	Tangential-momentum-coefficient
σ_T	Thermal-momentum-coefficient
t	Time
T	Gas temperature
T_0	Reference temperature
u	Gas velocity in x-direction
u_0	Reference velocity
v	Gas velocity in y-direction
V_c	Combustion rate

Introduction

The concept of microspacecraft became popular due to ongoing efforts by NASA to minimize the life cycle cost for outer space mission satellites by reducing the mass and the overall dimensions of the these satellites. Microspacecrafts have proven to be more versatile when it comes to accurate global positioning and greatly increases the mission flexibility.

Microspacecrafts may be classified into three categories based on their mass, size and power ranges.[1] A microspacecraft of characteristic dimension 30-40 cm and

---

[*] Graduate Student, Email: raju8515@kettering.edu, AIAA Student member.
[†] Post-Doctoral Research Associate, Email: bpandey@kettering.edu, AIAA Member.
[‡] Assistant Professor, Email: sroy@kettering.edu, AIAA Associate Fellow.

mass between 4-20 kg is included in the Class I of microspacecrafts. The smaller range of microspacecrafts with a typical dimension of the order of 10 cm and mass of above 1 kg constitute the Class II, while those less than 1 kg with dimension 3 mm or less falls into Class III category.

The demand for on-board propulsion system that would reduce the aerodynamic drag, neutralize the gravity-well distortion and generate precise altitude control is growing with rapid advancement in on-board technology.[2] The requirement for accurate navigational control for these satellites led to the development of micropropulsion systems, providing a thrust lower than 100μN.

Since the introduction of Field Emission Electric Propulsion (FEEP) thrusters,[3] several other microthrusters have been developed that meet the low thrust requirement. Examples include cold gas thrusters, vaporizing gas thrusters and chemical microthrusters. Besides the experimental reports,[3, 4] several researchers have investigated microthrusters using Navier-Stokes and DSMC models for various ranges of Reynolds number ranging from 1-10000.[2-3, 5] To predict the flow behavior of the gas inside the thruster, performance evaluation of supersonic cold gas thrusters have been done by Bayt et al [2,3]and Ivanov et al[5].

In general, fluids are modeled using either the continuum or the molecular approach. The continuum approach is used widely for fluid flow applications; however as the length scale of a physical system decreases, the validity of the standard continuum approach with no-slip boundary conditions diminishes. The local value of the Knudsen number determines the degree of appropriateness of the continuum model and is defined as,

$$Kn = \frac{\ell}{L} \qquad (1)$$

where ℓ is the mean free path of the fluid and L is the length scale of the physical system.

Knudsen number can also be written based on the relation between the Mach number and the Reynolds number as,

$$Kn = \sqrt{\frac{\pi\gamma}{2}}\frac{\mathrm{Ma}}{\mathrm{Re}} \qquad (2)$$

The local Knudsen number is a measure of the degree of rarefaction of gases encountered in small flows like in microelectromechanical system (MEMS) devices. *Fig 1* describes the different regimes depending on the Knudsen Number. As *Kn* increases, the rarefaction effects become more pronounced and eventually the continuum approach breaks down altogether.

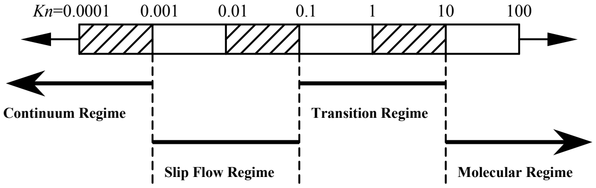

Fig 1: *Knudsen number regimes*

$Kn \to 0$: Euler Equations

$Kn \le 10^{-3}$: Navier Stokes equations with no-slip conditions (continuum regime)

$10^{-3} \le Kn \le 10^{-1}$: Navier Stokes equations with slip boundary (slip flow regime)

$10^{-1} \le Kn \le 10$: Transition regime

$Kn \ge 10$: Molecular regime

Rossi et. al[6] have introduced a one-dimensional (1-D) numerical model of the solid propellant combustion thruster developed by the French researchers at LAAS-CNRS. This thruster operates at subsonic speed and delivers a low thrust level for a few hundred milliseconds. The 1-D model solves Navier-Stokes equations based on method of lines and assumes no-slip continuum regime. Extending this effort, the present paper documents a two-dimensional (2-D) finite element formulation of the thruster based on the continuum no-slip wall condition. The 2-D solutions are compared with the reported 1-D results of Rossi et. al.[6]

As a second case, this paper also aims to model the flow through the micro nozzle by implementing the tangential-momentum-coefficient and the thermal-momentum-coefficient to accommodate for the slip flow and the temperature jump at the walls. This would be based on the assumption that the range of the Knudsen number lies between 0.001 – 0.1.

Thruster Model

Nozzle Geometry

The microthruster chosen for analysis uses a glycidyle azide polymer (GAP) based propellant for providing the thrust impulse developed by LAAS-CNRS.[7]

The basic structure of the microthruster consists of three sections: an array of Si-micromachined igniters consisting of patterned heaters serving as the exhaust for the combustion gases, an array of ceramic propellant tanks in the shape of a nozzle, and a thin glass wafer at the bottom of the tanks.

The combustion process begins when the propellant is ignited with a very small hot point at 260°C. The thin film of the dielectric resistor in the Si-micromachined igniters then breaks down and the gas exits from the thruster with a high velocity.

Figure 2 describes the converging-diverging nozzle geometry of the thruster used for the present analysis with following dimensions,

$L_1 = 3$ mm, $A_1 = 4\pi$ mm^2
$L_2 = 1$ mm, $A_1/A_2 = 5$
$L_3 = 4$ mm, $\alpha = 12^o$

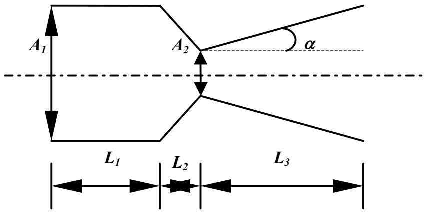

Fig.2 *Si-micromachined Microthruster*

The assumptions made for this particular analysis are,

1. The combustion products are gaseous and homogeneous.
2. The gas obeys the perfect gas law since at high temperature the gas is above its saturation conditions.
3. The thermal losses through the ceramic walls are negligible.
4. There are no shock waves or discontinuities in the low thrust system.

Properties of the gas are,

Parameter	***Value***
Combustion Temperature ,T_c	1800°C
Specific Heat at Const. Pressure, C_p	1835 J/kg K
Solid Propellant Density , ρ_p	1528 kg/m^3
Combustion Rate , V_c	7x10^{-3} P$^{0.6}$ m/s
Air Density, ρ_0	1.22 kg/ m^3
Reduced Gas Constant ,R	352.5 J/Kg K
Pressure at the Exit, P	1.01 x 10^5 Pa

Governing Equations

The standard 2-D Navier-Stokes equations governing the nozzle flow can be written as,

Conservation of Mass:

$$\frac{\partial \rho}{\partial t} + \frac{\partial \rho u}{\partial x} + \frac{\partial \rho v}{\partial y} = 0 \tag{3}$$

Conservation of x- momentum:

$$\frac{\partial \rho u}{\partial t} + u\frac{\partial \rho u}{\partial x} + v\frac{\partial \rho u}{\partial y} = -\frac{\partial P}{\partial x} + \mu\left(\frac{\partial^2 u}{\partial x^2} + \frac{\partial^2 u}{\partial y^2} + \frac{1}{3}\left(\frac{\partial^2 u}{\partial x^2} + \frac{\partial^2 v}{\partial x \partial y}\right)\right) \tag{4}$$

Conservation of y- momentum:

$$\frac{\partial \rho v}{\partial t} + u\frac{\partial \rho u}{\partial x} + v\frac{\partial \rho v}{\partial y} = -\frac{\partial P}{\partial y} + \mu\left(\frac{\partial^2 v}{\partial x^2} + \frac{\partial^2 v}{\partial y^2} + \frac{1}{3}\left(\frac{\partial^2 v}{\partial y^2} + \frac{\partial^2 u}{\partial x \partial y}\right)\right) \tag{5}$$

Conservation of energy:

$$\rho Cp\frac{DT}{Dt} = \frac{DP}{Dt} + \frac{\partial}{\partial x}\left(k\frac{\partial T}{\partial x}\right) + \frac{\partial}{\partial y}\left(k\frac{\partial T}{\partial y}\right) + \mu\left(2\left(\frac{\partial u}{\partial x}\right)^2 + 2\left(\frac{\partial v}{\partial y}\right)^2 + \left(\frac{\partial v}{\partial x} + \frac{\partial u}{\partial y}\right)^2 - \frac{2}{3}\left(\frac{\partial u}{\partial x} + \frac{\partial v}{\partial y}\right)^2\right) \tag{6}$$

The Pressure is defined using the perfect Gas law,

$$P = \rho RT \tag{7}$$

Equations (3)-(6) can be non-dimensionalized using averaged streamwise velocity u_0 at the exit for velocities u and v; dimensions x and y by reference length L, density ρ and pressure P by outlet conditions ρ_0 and P_0 respectively; and temperature T by reference temperature T_0. The normalized forms of equations (3)-(6) become,

Conservation of Mass:

$$\frac{\partial \rho^*}{\partial t^*} + \frac{\partial \rho^* u^*}{\partial x^*} + \frac{\partial \rho^* v^*}{\partial y^*} = 0 \tag{8}$$

Conservation of x- momentum:

$$\frac{\partial \rho^* u^*}{\partial t^*} + u^*\frac{\partial \rho^* u^*}{\partial x^*} + v^*\frac{\partial \rho^* u^*}{\partial y^*} = -\frac{\partial P^*}{\partial x^*} + \frac{\mu^*}{\mathrm{Re}}\left(\frac{\partial^2 u^*}{\partial x^{*2}} + \frac{\partial^2 u^*}{\partial y^{*2}} + \frac{1}{3}\left(\frac{\partial^2 u^*}{\partial x^{*2}} + \frac{\partial^2 v^*}{\partial x^* \partial y^*}\right)\right) \tag{9}$$

Conservation of y- momentum:

$$\frac{\partial \rho^* v^*}{\partial t^*}+u^*\frac{\partial \rho^* v^*}{\partial x^*}+v^*\frac{\partial \rho^* v^*}{\partial y^*}=-\frac{\partial P^*}{\partial y^*}$$

$$+\frac{\mu^*}{\mathrm{Re}}\left(\frac{\partial^2 v^*}{\partial x^{*2}}+\frac{\partial^2 v^*}{\partial y^{*2}}+\frac{1}{3}\left(\frac{\partial^2 v^*}{\partial y^{*2}}+\frac{\partial^2 u^*}{\partial x^*\partial y^*}\right)\right) \qquad (10)$$

Conservation of energy:

$$\rho^* Cp^* \frac{DT^*}{Dt^*}=Ec\frac{DP^*}{Dt^*}+\frac{k^*}{\mathrm{Re.Pr}}\left(\frac{\partial^2 T^*}{\partial x^{*2}}+\frac{\partial^2 T^*}{\partial y^{*2}}\right)$$

$$+\frac{Ec\mu^*}{\mathrm{Re}}\left(2\left(\frac{\partial u^*}{\partial x^*}\right)^2+2\left(\frac{\partial v^*}{\partial y^*}\right)^2+\left(\frac{\partial v^*}{\partial x^*}+\frac{\partial u^*}{\partial y^*}\right)^2-\frac{2}{3}\left(\frac{\partial u^*}{\partial x^*}+\frac{\partial v^*}{\partial y^*}\right)^2\right) \qquad (11)$$

The superscript * in (8)-(11) denotes normalized variables.

For $10^{-3} \le Kn \le 10^{-1}$, first order slip boundary conditions have to be implemented in the momentum and energy equations. Maxwell[8] derived slip relations for dilute, monoatomic gases. For an ideal gas flow in the presence of wall-slip boundary condition is given as,

$$u_{gas}-u_{wall}=\frac{2-\sigma_V}{\sigma_V}\ell\left(\frac{\partial u}{\partial y}\right)_w$$

$$+\frac{3}{4}\frac{\mu}{\rho T_{gas}}\left(\frac{\partial T}{\partial x}\right)_w \qquad (12)$$

Corresponding temperature-jump relation was derived by von Smoluchowski[9] as

$$T_{gas}-T_{wall}=\frac{2-\sigma_T}{\sigma_T}\left[\frac{2\gamma}{\gamma+1}\right]\frac{\ell}{\mathrm{Pr}}\left(\frac{\partial T}{\partial y}\right)_w \qquad (13)$$

In (12)-(13), u_{gas} and T_{gas} are the velocity and temperature of the gas adjacent to the wall, while u_{wall} and T_{wall} are the wall velocity and wall temperature, respectively, and the subscript w denotes wall condition. The second term in the Eqn (12) is known as thermal creep, which generates slip velocity in the direction opposite to the increasing temperature.

The dimensionless form of (12) and (13) are given by Gad-el-Hak,[10]

$$u^*_{gas}-u^*_{wall}=\frac{2-\sigma_V}{\sigma_V}Kn\left(\frac{\partial u^*}{\partial y^*}\right)_w$$

$$+\frac{3}{2\pi}\frac{(\gamma-1)}{\gamma}\frac{Kn^2\,\mathrm{Re}}{Ec}\left(\frac{\partial T^*}{\partial x^*}\right)_w \qquad (14)$$

$$T^*_{gas}-T^*_{wall}=\frac{2-\sigma_T}{\sigma_T}\left[\frac{2\gamma}{(\gamma+1)}\right]\frac{Kn}{\mathrm{Pr}}\left(\frac{\partial T^*}{\partial y^*}\right)_w \qquad (15)$$

The first order slip conditions are applicable to Navier-Stokes equations when the Kn is in the range of 0.001-0.1. For Kn > 0.1, it is necessary to develop higher order slip velocity conditions as the continuum regime breaks down altogether. A higher order slip velocity has been derived by Beskok[11]. For our purpose however, *Kn* remains less than 0.1. Hence we would restrict slip to first order conditions.

Numerical Method

Finite element algorithms are used extensively in numerical modeling of fluid flow and heat transfer.[12,13] Recently, Roy and Pandey[14,15] have implemented it for analyzing the partially ionized gas flow inside a Hall thruster. In this paper, we extend the finite element formulation[14,15] to predict the performance of the GAP-based microthruster.

The finite element (FE) based modeling allows for easy implementation of boundary conditions. Equations (8)-(11) may be expressed as $L(\mathbf{U})=0$, where $\mathbf{U} = (u, v, T, \rho)$ and L is a differential operator. The weak statement underlines the development of the range of CFD algorithms. Such an integral statement associated with eqns (8)-(11) is

$$\int_{\Omega} wL(\mathbf{U})d\Omega = 0 \qquad (16)$$

where w denotes any admissible test function.[12] Thereafter, the finite element (FE) spatial semi-discretization of the domain Ω of (11)-(18) employs the mesh $\Omega_e = \cup_e \Omega_e$ and Ω_e is the generic computational domain. Using superscript "*h*" to denote "spatial discretization," the FE weak statement implementation for (16) defines the approximation as

$$u(x_j) \approx u^h(x_j) = \bigcup_e u_e(x_j)$$

$$\text{and} \quad u_e(x_j) = N_k \mathbf{U}_e \qquad (17)$$

where subscript e denotes elements, and the trial space FE basis set $N_k(x_j)$ typically contains Chebyshev, Lagrange or Hermite interpolation polynomials complete to degree k, plus perhaps "bubble functions".[13] The spatially semi-discrete FE implementation of the *weak statement* WS^h for (17) leads to

$$W S^h = S_e \left(\int_{\Omega_e} N_k L_e(\mathbf{U})\, d\tau \right) \tag{18}$$

S_e symbolizes the "assembly operator" carrying local (element) matrix coefficients into the global arrays. Application of Green-Gauss divergence theorem in (18) will yield natural homogenous Neumann boundary conditions and the surface integral that contains the unknown boundary fluxes wherever Dirichlet (fixed) boundary conditions are enforced.

Independent of the physical dimension of Ω, and for general forms of the flux vectors, the semi-discretized weak statement of (18) always yields an ordinary differential equation (ODE) system:

$$M \frac{dU}{dt} + R(U) = 0 \tag{19}$$

where U(t) is the time-dependent finite element nodal vector. The time derivative *dU/dt,* is generally replaced by using a θ-implicit or τ-step Range-Kutta time integration procedure. In (19), M = S_e(M$_e$) is the "mass" matrix associated with element level interpolation, R carries the element convection information and the diffusion matrix resulting from genuine (not for Euler) or numerical elemental viscosity effects, and all known data. For steady state, (19) is usually solved using a Newton-Raphson scheme:

$$\mathbf{U}^{i+1}_{\tau+1} = \mathbf{U}^{i}_{\tau+1} + \Delta\mathbf{U}^{i} = \mathbf{U}_{\tau} + \sum_{p=0}^{i} \mathbf{U}^{p+1}, \tag{20}$$

$$\text{where } \Delta\mathbf{U}^i = -\left[\mathbf{M} + \theta\Delta t(\partial\mathbf{R}/\partial\mathbf{U})\right]^{-1} \mathbf{R}(\mathbf{U})$$

The obvious numerical issues will be associated with calculation of the "Jacobian" ∂R/∂U and inversion of the M+$\theta\Delta t$(∂R/∂U) matrix with sufficient accuracy. Here, an implicit (θ=1) time stepping procedure is employed.

The choice of time step is dictated by the Courant-Fredrich-Levy condition.[16] The code uses variable time steps till the transient features die down as the iteration converges to a steady state. The solution is declared convergent when the maximum residual for each of the state variable becomes smaller than a chosen convergence criterion of $\in=10^{-4}$. Here, the convergence of a solution vector U on node j is defined as the norm:

$$\frac{\|\mathbf{U}_j - \mathbf{U}_{j-1}\|}{\|\mathbf{U}_j\|} \le \in \tag{21}$$

Results and Discussions

The governing equations (8)-(11) have been solved using fully implicit (θ =1) numerical procedure. The computational nozzle geometry is discretized using 504 two-dimensional 9-node biquadratic finite elements.

No-slip Benchmarking

For the first case, the flow has been analyzed for a cross section ratio of $A_c/A_t = 5$ and the divergence angle of $\alpha = 12^o$ at steady state and compared with results by Rossi et. al.[6] For this model continuum approach has been used with no-slip wall boundary conditions. Based on the assumption that heat loss through the wall is negligible, walls are set to be at homogeneous Neumann condition.

The velocity u at the inlet is generated by the combustion processes and is directly proportional to the mass consumption rate of the propellant, $\rho_p V_c$. Gas is assumed to be axially directed at the inlet, i.e., v=0. Temperature at the inlet remains close to the combustion temperature of 1800 K and there is an approximate drop of 100 K inside the microthruster. Since the gas expands at the atmospheric pressure at the exit, the exit pressure P is set to be atmospheric.

For the given thruster specifications and dimensions the velocity of the gas in Fig 3 shows a peak at the throat and then drops down in the diverging part. While the peak in the centerline velocity distribution (Fig. 3a) is comparable with the reported 1-D result of Rossi et al,[6] a variation in the velocity distribution is noticeable both upstream and downstream of the throat. This behavior is indicative of the crosswise diffusion that is accommodated in our 2-D computation (Fig. 3b).

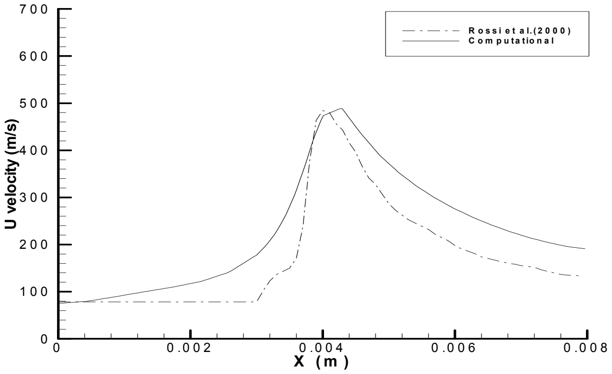

Fig. 3a *U Velocity (m/s) as a function of the length of the nozzle*

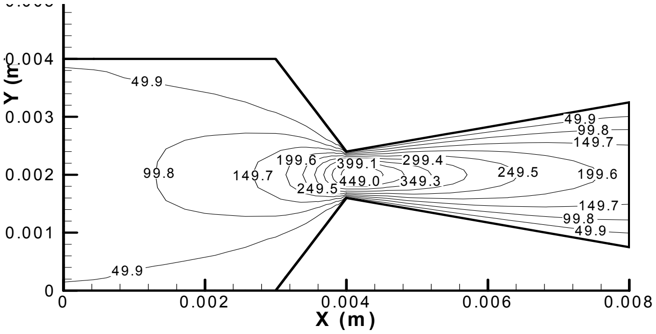

Fig. 3b *U Velocity (m/s) contours along the microthruster.*

The temperature is computed by specifying boundary conditions at thruster inlet and exit locations based on the assumption that there is only a temperature drop of 100 K inside the microthruster. The temperature of the gas at the inlet remains close to the combustion temperature and shows a gradual drop towards the exit, *Fig 4a and b*.

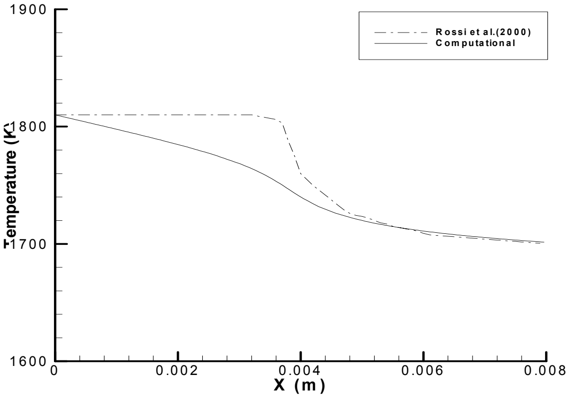

Fig.4a *Temperature (K) distribution along the nozzle centerline*

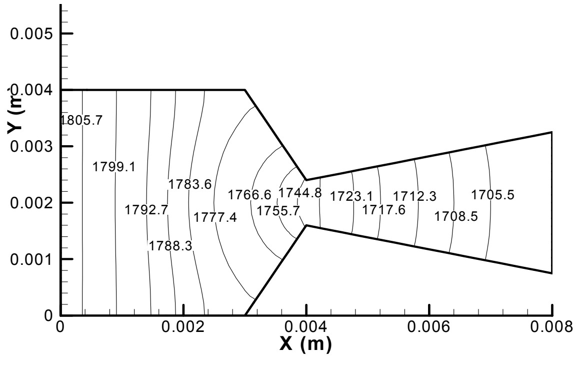

Fig. 4b *2-D Temperature (K) contour along the microthruster.*

The pressure is computed by specifying the boundary condition at the exit, which is set to be atmospheric. The pressure drop at the throat as shown in *Fig. 5* corresponds to the increase in the velocity near the throat. Further pressure drop downstream of the throat corresponds to the decrease in the density. This is expected from the mass conservation equation. The computed pressure ratio for the particular set of conditions is much below the critical pressure ratio for the GAP-based microthruster is 0.53 exhibiting a shockless transition at the throat.[6]

The mass flow rate distribution in *Fig. 6* exhibits a sharp rise along the length of the microthruster till the throat and then drops down since the flow is subsonic and the gas expands in the diverging part, *Fig 8*. The mass flow rate depends on the variation in density and velocity and since the pressure in the thruster nearly remains atmospheric it shows a similar profile to the velocity.

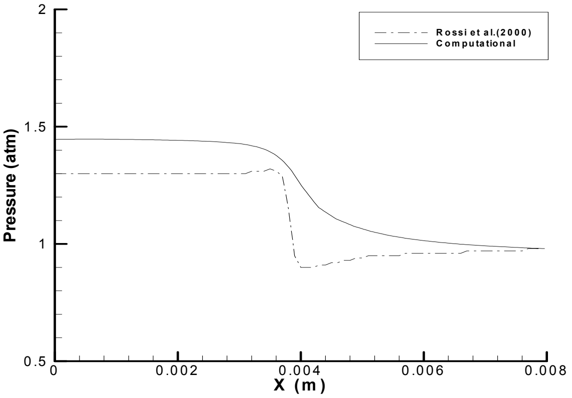

Fig. 5 *Pressure (atm) as a function of the length of the nozzle*

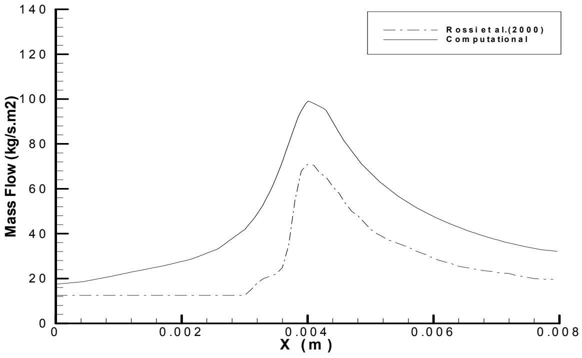

Fig. 6 *Mass flow rate (kg/sec. m ^{2}) as a function of the length of the nozzle*

Fig 7 shows that for the subject flow conditions, the flow through the micronozzle remains subsonic with the Mach number well below 1 at the throat. For this subsonic case the expansion of gas causes the drop of Mach number at the outlet, *Fig 7*. Increasing the inlet to throat ratio would however, further increase the velocity at the throat causing the rise in Mach number possibly making the flow supersonic.

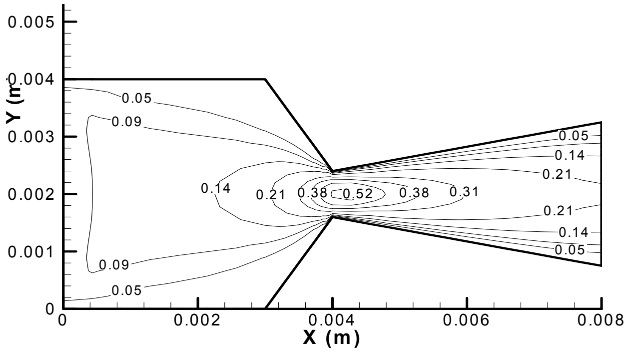

Fig. 7 *2-D Mach number contour along the microthruster.*

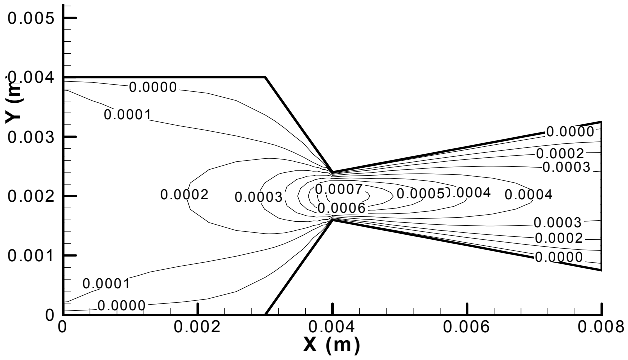

Fig. 8 *Knudsen number contours inside the microthruster.*

The Knudsen number contours in *Fig 8*, indicate a peak below 10^{-3} at the nozzle throat indicating the validity of applying no-slip boundary conditions to the present case study.

Corresponding reaction thrust T_e due to the ejection of hot gas at high velocity may be computed as a function of the average exhaust fluid velocity u_{ex}, mass flow rate $\dot{m}$ of the gas, exit area A_e and the pressure differential (P_{ex}–P_e) at the exit of the nozzle, i.e.,

$$T_e = \dot{m} \times u_{ex} + \left(P_{ex} - P_e\right) A_e \qquad (22)$$

Assuming the exhaust pressure P_{ex} is equal to the exit pressure P_e, the thrust becomes $T_e = \dot{m} \times u_{ex} = \rho_{ex} u_{ex}^2 A_e$. For the subject GAP microthruster, the thrust predicted from the 2-D simulation is 33.3 mN that is 44% higher than the 1-D prediction of approximately 23 mN.[6]

Slip Wall Comparison

For the second case, the thruster was modeled with the second set of boundary conditions and the eqns (14)-(15) implemented for solving the slip boundary conditions.

For the second case, the slip-boundary with temperature jump wall condition is implemented using the tangential-momentum coefficient σ_V and the temperature-momentum coefficient σ_T at the walls. These coefficients indicate the fraction of the molecules reflected diffusively from the walls. For σ_v =0 the molecules reflect specularly indicating the reversal in their normal velocity due to normal momentum transfer to the wall. For σ_v = 1 the molecules reflect diffusively when reflected from the wall with zero tangential velocity.

The value of the coefficients σ_V and σ_T depends on the surface finish, the fluid, temperature, and local pressure. The value of $\sigma_V \approx 0.80$ for nitrogen, argon or carbon dioxide in a silicon micromachined channel has been determined experimentally by Arkilic.[17] Here, we assume $\sigma_V = \sigma_T \approx 1.0$ for convenience.

For the comparison between slip wall and no-slip wall cases, the boundary conditions are specified as follows. The velocity u at the inlet is specified to be 50 m/s. Gas is assumed to be axial directed and hence at the inlet v=0. Temperature T at the inlet is considered to be lower than the first case and is set to be 290 K, there is an overall drop of 18 K in the domain. This temperature condition will guarantee a higher Kn value so that the slip wall condition may be applied. Like the previous case, at the outlet the gas expands to atmospheric pressure.

For the given inlet conditions for this thruster, the velocity picks up at the throat and drops down in the diverging part. *Fig 9a*, shows the slip flow at the walls gives a slightly lower peak velocity than the no-slip condition. Comparisons of the u-velocities in the radial-direction at three distinct locations along the length of the micro thruster show that the effect of the slip boundary conditions becomes predominant with higher velocity, which in this case is at the throat, *Fig 9b*. Since the gas expands and the velocity drops in the diverging part the difference in velocities shows up more at the throat than either in the chamber or in the divergent part. *Fig 9c* clearly documents this difference in the zoomed in velocity maxima at the throat location, x = 0.004m.

Fig. 10 documents that for the same inlet flow velocity, less pressure drop is required in slip wall boundary to maintain the flow due to reduced wall shear for slip condition as compared to the no-slip case. This effect is clearly visible with lower pressure ratio requirement for the slip wall case.

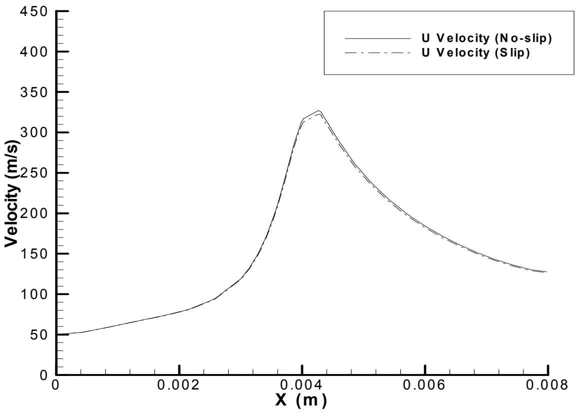

Fig. 9a *U Velocity (m/s) comparison for the slip and no-slip conditions as a function of the length of the nozzle*

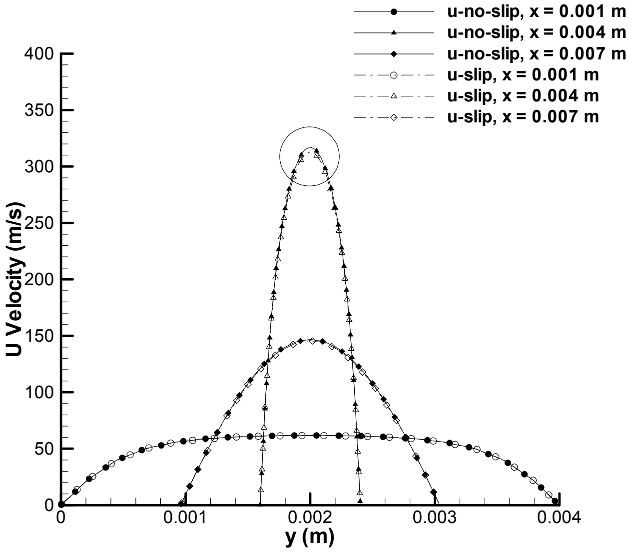

Fig. 9b *The u- velocity (m/s) for the slip and no-slip conditions at various points along the length of the microthruster*

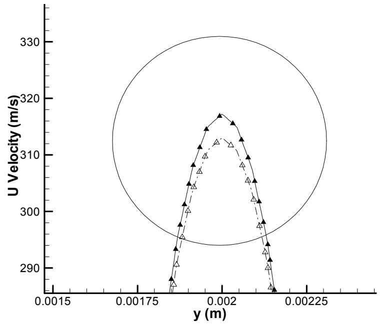

Fig. 9c *Zoomed in velocity comparison at the throat location (x=0.004m) for the slip and no-slip conditions.*

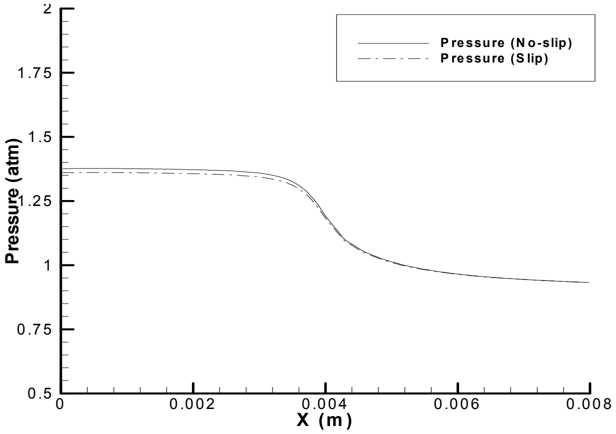

Fig.10 *Comparison of pressure (atm) distribution for the slip and no-slip conditions as a function of the length of the nozzle.*

However, as shown in Fig. 11, the temperature profiles for both the slip and the no slip case remains largely the same. The slip condition result shows a lower mass flow rate than the no-slip condition since the mass flow rate is predominantly dependent on the inlet velocity, *Fig 12*.

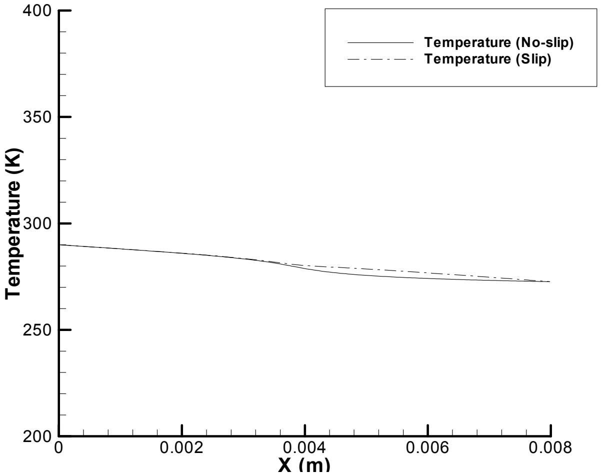

Fig.11 *Temperature (K) for the slip and no-slip conditions as a function of the length of the nozzle.*

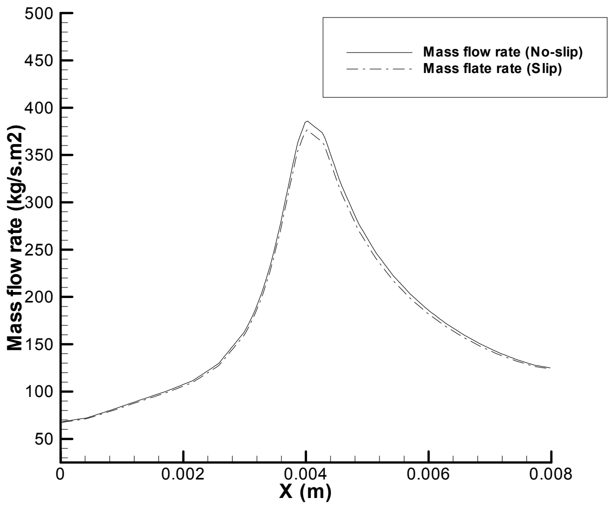

Fig.12 *Mass flow rate (kg/s.m2) for the slip and no-slip conditions as a function of the length of the nozzle.*

For the given set of conditions the Mach number at the throat is the highest, but since the flow is subsonic the mach number drops in the diverging part due to the expansion of the gas, *Fig 13*. The slip flow condition would show a higher mach number due to the relatively high velocity generated.

The Knudsen number regime, *Fig 14,* shows that Knudsen number nearer to the throat falls under the slip flow regime. But in this case since the Knudsen number is very near to the lower limit of the no-slip regime, the effect of the slip condition is minimal, and the results with continuum assumption would show marginal error in the solution.

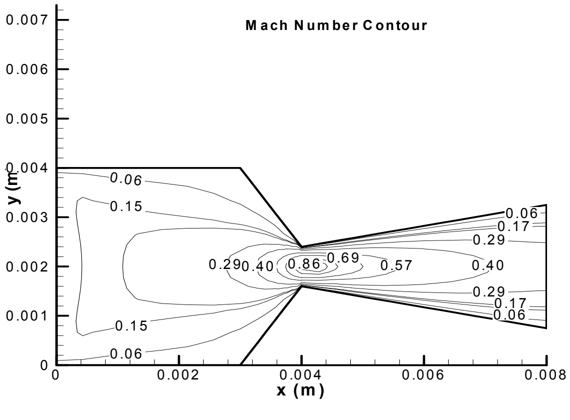

Fig.13 *Mach Number contours for the slip conditions along the microthruster.*

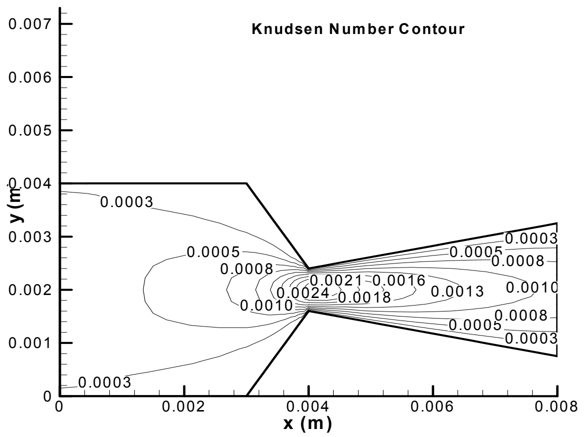

Fig.14 *Knudsen Number contours for the slip conditions along the microthruster.*

Conclusions

A 2-D model has been developed using finite element methodology for analyzing the flow along a microthruster. Numerical results are comparable to a published 1-D study. The 2-D model gives better details of the flow inside the micronozzle and can be helpful in understanding the physics and predicting the thrust. The model includes slip and no-slip boundary conditions for appropriate Knudsen number range. Documented results show a small difference for low Kn (<0.003). This indicates that for higher Knudsen number in cold microthrusters the difference would be higher as the continuum regime increasingly breaks down.

References

[1] Mueller J., 1997, "Thruster options for microspacecrafts: A review and evaluation of existing hardware and emerging technologies." *33rd AIAA/ASME/SAE/ASEE Joint Propulsion Conference & Exhibit, July 1997, AIAA97-3058.*

[2] Bayt R.L., Breuer K., 2001, "Systems Design and Performance of Hot and Cold Supersonic Microjets.*" 39th AIAA Aerospace Science Meeting and Exhibit, January 2001, AIAA-2001-0721.*

[3] Bayt R.L., Ayon A.A. and Breuer K, 1997, "A Performance Evaluation of MEMS based Micronozzles," *33rd AIAA/ASME/SAE/ASEE Joint Propulsion Conference and Exhibit, July 1997, AIAA97-3169.*

[4] Grisnik, S.P., Smith, T.A. and Salz, L.E., 1987, "Experimental Study of Low Reynolds Number Nozzle" *AIAA Paper 87-0092.*

[5] Ivanov M.S., Markelov G.N., Ketsdever A.D , Wadsworth D.C., 1999, "Numerical Study of Cold Gas

Micronozzle Flow," *37th Aerospace sciences Meeting & Exhibit, January 1999, AIAA99-0166.*

[6]Rossi C., Rouhani M.D. and Estève D., 2000, "Prediction of the performance of a Si-micromachined microthruster by computing the subsonic gas flow inside the thruster." *Sensors and Actuators, Physical A, vol.87, pp. 96-104.*

[7]Rossi, C., Estéve, D., Fabre, N., Do Conto, T. and Conédéra, V., 1999, "New generation of MEMS-based microthrusters for microspacecrafts applications" *Conference on Micro & Nano Technologies for Space applications, Pasadena, CA, April 1999.*

[8]Maxwell, J.C., 1879, "On stresses in Rarefied Gases arising from Inequalities of Temperature." *Philosophical Transactions of the Royal Society Part 1, vol. 170, pp. 231-256.*

[9]Smoluchowski, von M., 1898, "Ueber Wärmeleitung in verdünnten Gasen." *Annalen der Physik und Chemi,, vol. 64, pp. 101-130..*

[10]Gad-ek-hak, M., 1999, "The Fluid Mechanics of Microdevices- The Freeman Scholar Lecture." *Journal of Fluids Engineering, vol.121, pp. 5-33.*

[11]Beskok, A., 1994, "Simulation of Heat and Momentum Transfer in Complex Micro-geometries."*, Princeton Univeristy, M.Sc. Thesis.*

[12]Oden, J.T. and Oliveira, E.R.A., 1976, "Lectures on Finite Element Methods in Continuum Mechanics" *The University of Alabama in Huntsville Press, Huntsville.*

[13]Roy, S. and Baker, A.J., 1998, "Numerical Heat Transfer – Part B."*, Vol. 33, vol. 33, no. 1, pp. 5-36.*

[14]Roy S. and Pandey, B.P.,2002, "Plasma-Wall Interaction inside a Hall Thruster." *Journal of Plasma Physics (to appear).*

[15]Roy S. and Pandey, B.P., 2002, "Numerical Investigation of a Hall Thruster Plasma." *Physics of Plasmas (in press, AIP ID # 031209PHP).*

[16]Richtmyer, R.D. and Morton, K.W., 1967, "Difference Methods for Initial-Value Problems."*,2nd Ed, Interscience Publishers, Wiley, New York.*

[17]Arkilic, E.B., 1997, "Measurement of the Mass Flow and Tangential Momentum accommodation coefficient in silicon micromachined channels." *MIT, Ph.D. Thesis.*